PHOTONICS Research

Negative refraction of ultra-squeezed in-plane hyperbolic designer polaritons

Qiaolu Chen,[1,2] Yihao Yang,[1,2,5] Li Zhang,[1,2] Jialin Chen,[1,2] Min Li,[1,2] Xiao Lin,[1,2] Rujiang Li,[3,4] Zuojia Wang,[1,2] Baile Zhang,[3,4,6] and Hongsheng Chen[1,2,7]

[1]Interdisciplinary Center for Quantum Information, State Key Laboratory of Modern Optical Instrumentation, ZJU-Hangzhou Global Scientific and Technological Innovation Center, Zhejiang University, Hangzhou 310027, China
[2]International Joint Innovation Center, Key Laboratory of Advanced Micro/Nano Electronic Devices & Smart Systems of Zhejiang, The Electromagnetics Academy at Zhejiang University, Zhejiang University, Haining 314400, China
[3]Division of Physics and Applied Physics, School of Physical and Mathematical Sciences, Nanyang Technological University, Singapore 637371, Singapore
[4]Centre for Disruptive Photonic Technologies, The Photonics Institute, Nanyang Technological University, Singapore 639798, Singapore
[5]e-mail: yangyihao@zju.edu.cn
[6]e-mail: blzhang@ntu.edu.sg
[7]e-mail: hansomchen@zju.edu.cn

Received 10 March 2021; revised 30 May 2021; accepted 14 June 2021; posted 15 June 2021 (Doc. ID 424739); published 29 July 2021

The in-plane negative refraction of high-momentum (i.e., high-k) photonic modes could enable many applications such as imaging, focusing, and waveguiding in a planar platform at deep-subwavelength scales. However, its practical implementation in experiments remains elusive so far. Here we propose a class of hyperbolic metasurfaces, which is characterized by an anisotropic magnetic sheet conductivity and can support the in-plane ultra-high-k magnetic designer polaritons. Based on such metasurfaces, we report the experimental observation of the all-angle negative refraction of designer polaritons at extremely deep-subwavelength scales. Moreover, we directly visualize the designer polaritons with hyperbolic dispersions. Importantly, for these hyperbolic polaritons, we find that their squeezing factor is ultra-large. To be specific, it can be up to 129 in the experiments, an ultra-high value exceeding those in naturally hyperbolic materials. This work may pave a way toward exploring the extremely high confinement and unusual propagation of magnetic designer polaritons over monolayer or twisted bilayer hyperbolic metasurfaces.

https://doi.org/10.1364/PRJ.424739

1. INTRODUCTION

Three-dimensional hyperbolic media are characterized by the anisotropic permittivity or permeability tensor, with a principal component being opposite in sign to the other two principal components [1–6]. One of the most important properties of hyperbolic media is that they support photonic modes with high momentum [1 order larger than photons' momentum in free space (denoted as k_0)], allowing for confining photons at deep-subwavelength scales. The high-momentum or high-k modes play a crucial role in many applications of hyperbolic media [5], such as low-threshold Cherenkov radiation [7,8], enhanced spontaneous emission [9], super-Planckian thermal emission [10,11], ultra-sensitive sensors [12], and subwavelength imaging [13]. Recent research has revealed that such high-k modes also exist in ultra-thin hyperbolic media, or two-dimensional (2D) hyperbolic media, such as hyperbolic metasurfaces (e.g., nanostructured van der Waals (vdW) materials [14], designed metal-based metasurfaces [15–19]), and slabs of naturally hyperbolic materials [20] (e.g., the uniaxial boron nitride (BN) [21–23], the biaxial vdW crystal α-MoO_3 [24,25]).

Realization of in-plane negative refraction of high-k modes is of great significance and interest due to its unique applications such as imaging, focusing, and waveguiding in a planar platform at deep-subwavelength scales [26–28]. Such a goal has become a possibility, thanks to the advent of artificial hyperbolic metasurfaces and naturally hyperbolic materials. Though the negative refraction of hyperbolic surface plasmon polaritons (SPPs) was previously experimentally demonstrated at an interface between a hyperbolic metasurface and a flat silver film, both the SPPs on the silver film and hyperbolic metasurface are relatively weakly confined (their wave vectors are usually less than $3k_0$) [16]. This approach cannot directly apply to the high-k modes, as the high-k surface-wave modes are usually strongly reflected or scattered when coupling to low-k modes (such as SPPs on the silver film), owing to the large in-plane

and out-of-plane momentum mismatching [29]. Therefore, to achieve in-plane negative refraction of high-k modes, the dispersions in both regions need to be precisely engineered. One straightforward way to do so is to employ two materials/structures supporting high-k modes with opposite group velocities. For example, graphene supports high-k plasmon polaritons with positive group velocity, and BN supports high-k phonon polaritons with negative group velocity in its first reststrahlen band [27]. Moreover, by judiciously tuning the chemical potential of graphene and the thickness of BN, it is possible to flexibly flip the sign of the group velocity of the hybrid polaritons in graphene–BN heterostructures. As such, graphene–BN heterostructures can be a versatile platform to support the in-plane negative refraction of high-k modes. However, the operational frequency bandwidth of negative refraction in graphene–BN heterostructures is within the first reststrahlen band of BN and is thus very narrow. Such a strict requirement is then experimentally unfavorable and challenging. Recently, Jiang *et al.* proposed to realize the broadband all-angle negative refraction of high-k hyperbolic plasmon polaritons at an interface constructed by two identical nanostructured graphene metasurfaces with different rotation angles [28]. However, both fabrication and experimental characterization of such graphene metasurfaces are quite challenging. In short, although there are some theoretical proposals of in-plane negative refraction of high-k modes, their practical realization in experiments has not been reported so far.

To overcome the above challenges, we propose, design, and fabricate a class of hyperbolic metasurfaces characterized by an anisotropic magnetic sheet conductivity (denoted as σ_m) [30,31], which supports in-plane ultra-high-k magnetic designer polaritons [32]. Based on such metasurfaces, all-angle negative refraction of ultra-high-k designer polaritons is observed in the experiments [see Fig. 1(a)]. Moreover, our microwave measurements directly show that the designer polaritons indeed exhibit in-plane hyperbolic dispersions and have ultra-squeezed wavelength down to 129 times smaller than the free-space photons' wavelength (denoted as λ_0). Such an ultra-high

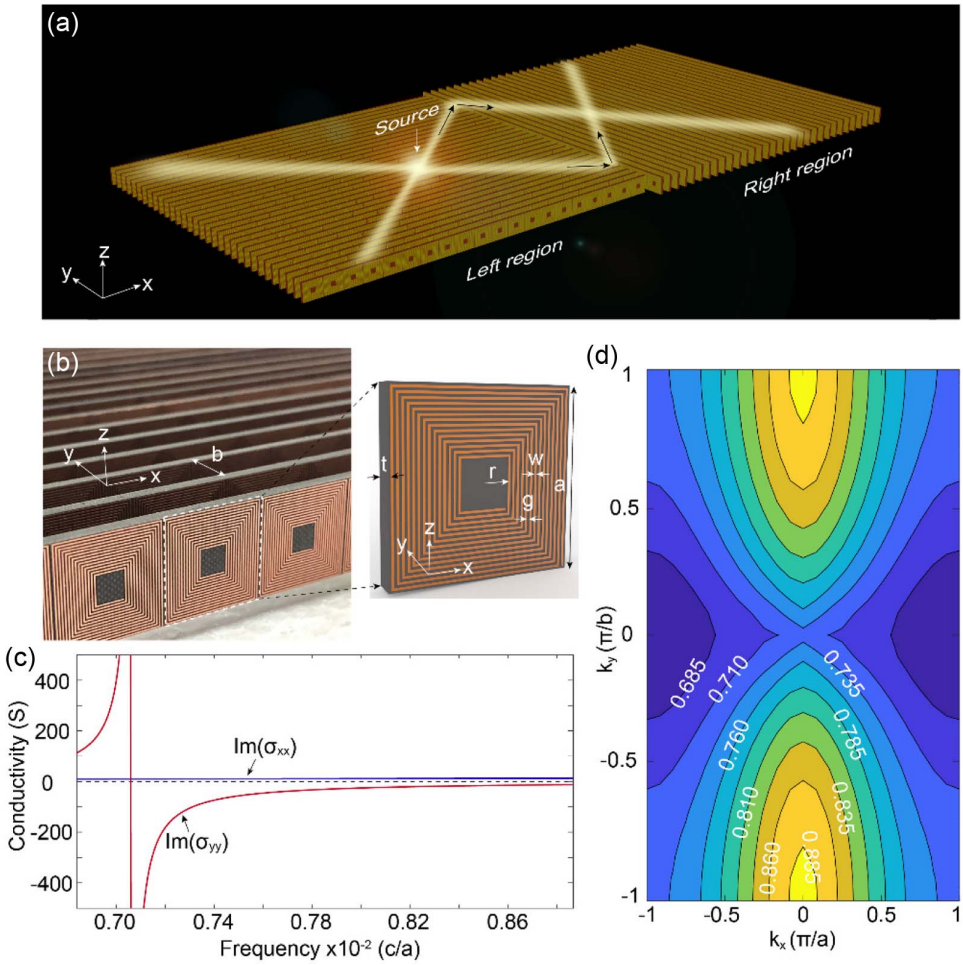

Fig. 1. Anisotropic-σ_m hyperbolic metasurface. (a) Schematic view of in-plane negative refraction based on the designed hyperbolic metasurface. The hyperbolic metasurface in the right region is rotated by 90°, comparing with the left one. The black arrows indicate the power flow. (b) Left panel: photograph of the fabricated sample. The sample is composed of arrays of coiling copper wires patterned on dielectric substrates. Right panel: details of a unit cell. Here, $a = 15.2$ mm, $b = 9$ mm, $r = 2$ mm, $t = 2$ mm, $w = 0.2$ mm, and $g = 0.2$ mm. The relative permittivity of the substrate is $3.5 + 0.001i$. The thickness of copper wires is 0.035 mm. The number of coil turns is 14. (c) Numerically-calculated $\mathrm{Im}(\sigma_m)$ of the metasurface. Blue (red) solid line represents values of $\mathrm{Im}(\sigma_{xx})$ [$\mathrm{Im}(\sigma_{yy})$]. Black dashed line denotes a value of zero. (d) Iso-frequency contours of the hyperbolic metasurface in the first Brillouin zone. The frequency values are normalized by $(c/a) \times 10^{-2}$.

squeezing factor (defined as λ_0/λ_p, where λ_p is the designer polaritons' wavelength, or k_p/k_0) exceeds those in naturally in-plane hyperbolic materials demonstrated previously (usually less than 60 in the experiments) [24,25]. Our work provides a distinctive way to achieve in-plane negative refraction of ultra-high-k modes, which could apply to other in-plane hyperbolic materials. Additionally, our metasurfaces are readily tailorable in frequency and space, which form a highly variable platform for exploring the extremely high confinement and unusual propagation of in-plane hyperbolic polaritons.

2. RESULTS

We start with the arrays of coiling copper wires patterned on dielectric substrates [see Fig. 1(b)], where the surface currents flowing along the spiral coils produce strong magnetic dipole moments vertical to the coils. An enlarged view of a unit cell is shown in the right panel of Fig. 1(b), where the gray region denotes the dielectric substrate with relative permittivity $\varepsilon_r = 3.5 + 0.001i$ and thickness $t = 2$ mm, and the orange region represents a 35-μm coiling copper wire with inner radius $r = 2$ mm, width $w = 0.2$ mm, gap $g = 0.2$ mm, and the number of coil turns $N = 14$. The periods are $a = 15.2$ mm (x axis) and $b = 9$ mm (y axis), respectively.

We then numerically calculate the iso-frequency contours (IFCs) of the fundamental mode of the proposed hyperbolic metasurface in the first Brillouin zone (FBZ) by employing the eigenvalue module of a commercial software Computer Simulation Technology (CST) Microwave Studio, as shown in Fig. 1(d). One can see that the IFCs are open hyperbolas from $0.735 \times 10^{-2}(c/a)$ to $0.885 \times 10^{-2}(c/a)$. Here, c is the velocity of light in free space. In addition, the magnetic field is highly confined in both the vertical and horizontal directions, indicating the surface-wave nature of the eigenmodes (see Appendix A). Also, the operational wavelength is around 2×10^3 mm, which is much larger than the thickness of the metasurface (i.e., 15.2 mm). Note that there are distortions in the hyperbolic dispersions near the edge of the first Brillouin zone. This is because the corresponding wavelength of designer polaritons is comparable with the size of the unit cell, and the metasurface cannot be described by the effective sheet conductivity model precisely.

To understand the behaviors of the designer polaritons over the metasurface, we model the proposed hyperbolic metasurface as a 2D magnetic sheet conductivity layer with infinitesimal thickness surrounded by two vacuum half-spaces [33,34]. Here we consider the hyperbolic metasurface as a lossless medium because ohmic losses of the substrate and copper are negligible at microwave frequencies. Then, by adopting a standard retrieval method [30], we extract the magnetic sheet conductivity of the metasurface:

$$\overline{\overline{\sigma_m}} = \begin{pmatrix} \sigma_{xx} & 0 \\ 0 & \sigma_{yy} \end{pmatrix}. \tag{1}$$

The resulting σ_m plot is shown in Fig. 1(c), where $\mathrm{Im}(\sigma_{xx})$ and $\mathrm{Im}(\sigma_{yy})$ are opposite in sign from $0.735 \times 10^{-2}(c/a)$ to $0.885 \times 10^{-2}(c/a)$, indicating a hyperbolic frequency band. The corresponding dispersion relation of the designer polaritons is

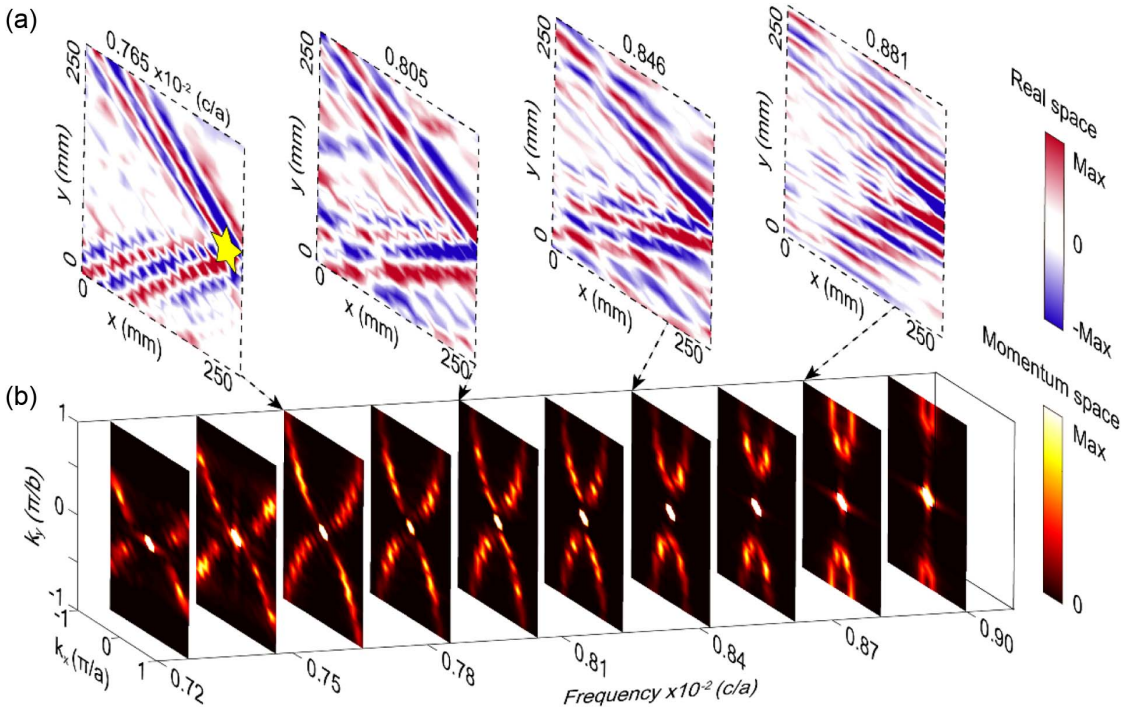

Fig. 2. Measured magnetic field distributions and iso-frequency contours. (a) Measured magnetic patterns of H_z field in the real space on the xy plane 3 mm over the hyperbolic metasurface at $0.765 \times 10^{-2}(c/a)$, $0.805 \times 10^{-2}(c/a)$, $0.846 \times 10^{-2}(c/a)$, and $0.881 \times 10^{-2}(c/a)$, respectively. The yellow star indicates the source position. The color bar measures the real part of H_z. (b) Iso-frequency contours in the momentum space obtained by applying spatial Fourier transform to the corresponding complex H_z field. The color bar measures energy intensity.

$$\frac{1}{\eta_0^2}(\sigma_{xx}k_x^2+\sigma_{yy}k_y^2)^2(k_x^2+k_y^2-k_0^2)+4k_0^2(k_x^2+k_y^2)^2=0, \quad (2)$$

where $k_{x,y}$ are the wave vectors in the xy plane and η_0 is the characteristic impedance of vacuum [33,35]. Note that, as transverse magnetic (TM) modes here are barely confined on the metasurface, we mainly focus on transverse electric (TE) modes with out-of-plane electric field and in-plane magnetic field. Here, the plane of incidence is formed by the normal to the boundary surface and the incident wave vector, which is vertical to the metasurface plane [28,33]. Comparing the analytical and simulated dispersions, we find a good agreement between them (see the Appendix C).

In the following, we carry out experiments to characterize the proposed hyperbolic metasurface. The experimental sample consists of 20 by 32 unit cells. To excite the designer polaritons efficiently, a port of the vector network analyzer (VNA) is directly connected to a coil unit cell at the edge of the metasurface. Another port of the VNA is connected to a detector that is a compact coil with a magnetic resonance around $0.806\times10^{-2}(c/a)$. The coil-like detector that oriented in the z-direction is fixed at a robotic arm of a moving platform and moves on the xy plane 3 mm above the metasurface. By scanning the sample, the complex magnetic patterns of H_z field (including phase and amplitude) are recorded. The size of the scanning region is approximately 250 mm by 250 mm, with a resolution of 15.2 mm by 9 mm. See the details of the experimental setup in the materials and methods.

The measured field patterns are shown in Fig. 2(a). One can directly observe the significant feature of hyperbolic designer polaritons, that is, concave polariton wavefronts. We note that weak reflection can be noticed from the measured field patterns [see the field pattern at $0.805\times10^{-2}(c/a)$ in Fig. 2(a)], owing to the finite size effect of the metasurface. For further proof of in-plane hyperbolic dispersions, we extract the IFCs in the momentum space by applying spatial Fourier transform to the corresponding complex field patterns [see Fig. 2(b)]. One can see that the measured IFCs are indeed hyperbola-like curves (see Appendix D), thus experimentally corroborating the simulated IFCs [Fig. 1(d)]. Note that there is a bright spot at the center of the FBZ at each frequency, which attributes to the radiation noise [19].

Next, we retrieve the squeezing factors of the hyperbolic designer polaritons, whose maximal value is determined by the period of the unit cell and the operational wavelength. As shown in Fig. 3(a), the squeezing factors of the in-plane polaritons are remarkably large, with a maximum value of 129 in both experiments and simulations, revealing the ultra-high-k nature of the hyperbolic designer polaritons. Note that compared with the squeezing factors in the previous in-plane hyperbolic metasurfaces or naturally in-plane hyperbolic materials such as vdW crystal α-MoO_3, which are usually less than 60 [24,25], the maximum squeezing factor achieved in our experiments is an ultra-high value. Figure 3(b) depicts the IFC directly obtained by applying spatial Fourier transform to the corresponding complex field pattern of H_z at $0.76\times10^{-2}(c/a)$ [Fig. 3(c)] where the squeezing factor is maximal.

Finally, we experimentally realize the in-plane negative refraction of the designer polaritons, based on the present anisotropic-σ_m hyperbolic metasurface. We first construct an interface consisting of two identical metasurfaces apart from a 90° rotation [see the schematic in Fig. 1(a)]. A point source is placed at the center of the left region, and hyperbolic designer polaritons with concave wavefronts are launched. Remarkably, the designer polaritons are negatively refracted at the interface, with the incident and refracted beams on the same side of the normal, as shown in Fig. 4(a). This intriguing phenomenon can be explained by the measured IFCs of both regions, as illustrated in Fig. 4(b). One can see that the directions of the y-component of group velocities (parallel to the interface) are opposite for incident and refracted polaritons, according to the conservation law where the tangential components of the wave vectors in left and right regions should be matched. As the group velocity determines the direction of power flow, negative refraction of designer polaritons occurs at the interface [28]. Note that parasitic noise can be spotted from the measured field patterns, owing to the reflection from the interface between two metasurfaces and from the metasurface edges.

Additionally, the negative refraction also occurs at other frequencies, e.g., $0.735\times10^{-2}(c/a)$, $0.765\times10^{-2}(c/a)$, $0.775\times10^{-2}(c/a)$, as shown in Fig. 4(c), which indicates

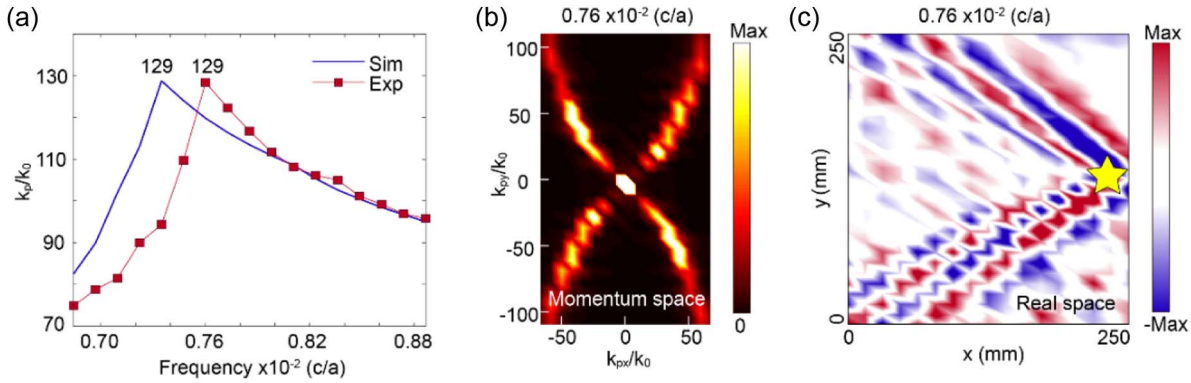

Fig. 3. Achieving an ultra-high squeezing factor in our hyperbolic metasurface. (a) Retrieved squeezing factors of the designer polaritons from simulated and experimental results. An ultra-high squeezing factor of 129 at $0.76\times10^{-2}(c/a)$ is observed. (b) Measured momentum space at $0.76\times10^{-2}(c/a)$. The color bar measures the energy intensity. (c) Measured H_z field on the xy plane 3 mm over the hyperbolic metasurface at $0.76\times10^{-2}(c/a)$. The excitation is marked as a yellow star. The color bar measures the real part of H_z.

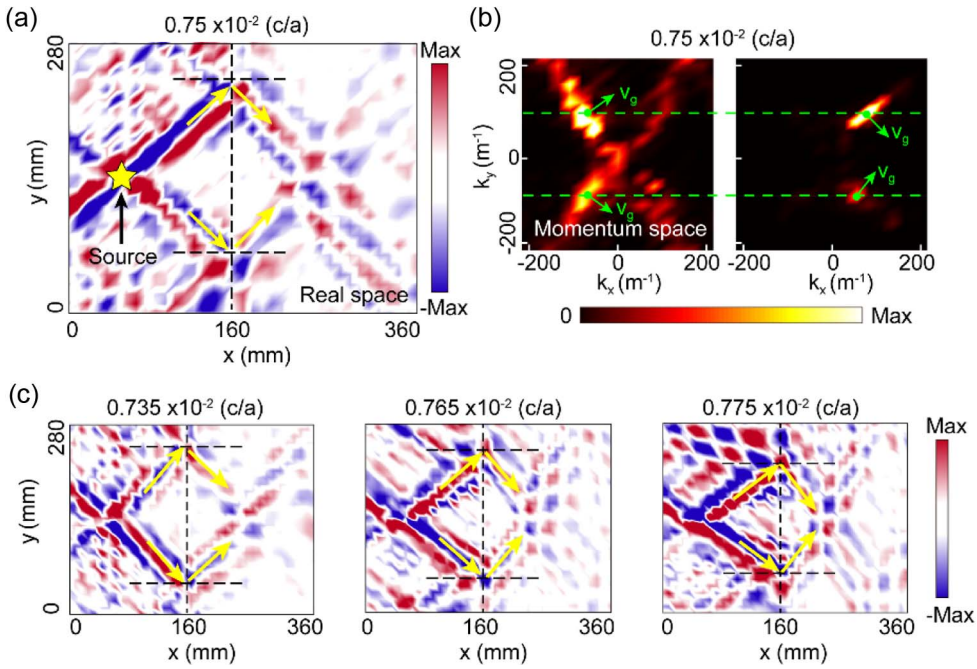

Fig. 4. Experimental validation of all-angle in-plane negative refraction of ultra-high-k designer polaritons. (a) Measured H_z field on the xy plane 3 mm above the hyperbolic metasurface at $0.75 \times 10^{-2}(c/a)$, indicating negative refraction. The vertical black dashed line denotes the interface. The horizontal black dashed lines are normals. The excitation is marked as a yellow star. The yellow arrows represent the directions of the power flow. The color bar measures the real part of H_z. (b) Measured momentum space of the hyperbolic designer polaritons in the left and right regions at $0.75 \times 10^{-2}(c/a)$, respectively. The green arrows indicate the directions of group velocities (power flow). The color bar measures energy intensity. (c) Measured H_z field at $0.735 \times 10^{-2}(c/a)$, $0.765 \times 10^{-2}(c/a)$, and $0.775 \times 10^{-2}(c/a)$, respectively.

the relatively broad operational bandwidth. We want to mention that for any designer polaritons launched in the left/right region, the negative refraction always happens at the interface regardless of the incidence angle. Therefore, we denote such a phenomenon as all-angle in-plane negative refraction [27,28,36,37]. We note that the negative refraction could not be observed at the frequency above $0.83 \times 10^{-2}(c/a)$, because the y-component momenta of the designer polaritons in two hyperbolic metasurfaces could not match with each other at higher frequencies.

3. DISCUSSION

We have thus proposed and experimentally identified a class of hyperbolic metasurfaces characterized by an anisotropic magnetic sheet conductivity, which supports ultra-high-k in-plane magnetic designer polaritons featuring with hyperbolic dispersions. Based on the proposed metasurface, all-angle in-plane negative refraction of the ultra-squeezed designer polaritons with good impedance matching is observed experimentally. Remarkably, an ultra-high squeezing factor of 129 is achieved in the experiments, which exceeds those in the naturally or artificially in-plane hyperbolic materials demonstrated previously. The present scheme for the achievement of negative refraction is also applicable to other natural materials and may enable intriguing applications. In addition, the present metasurfaces with highly squeezing factors and tunability could serve as an excellent platform to explore the applications and physics of in-plane hyperbolic polaritons. For example, it would be interesting to investigate the topological designer polaritons and magic angles in twisted bilayer hyperbolic metasurfaces [38–42]. By scaling down the unit cell, our design could apply to higher frequencies based on the modern nanofabrication technology (see the Appendix E), such as terahertz and far-infrared frequencies and may find many applications in flatland optics, e.g., waveguiding, imaging, and focusing [43,44]. As the hyperbolic polaritons in natural van der Waals materials are usually limited to optical and near-infrared frequencies, the present metasurface design working well from microwave to far-infrared frequencies could be excellently complementary to the naturally hyperbolic materials.

APPENDIX A: THE MAGNETIC FIELD DISTRIBUTIONS OF THE EIGENMODES

Figure 5 illustrates the field distributions of eigenmodes, which manifests that the magnetic field is highly confined in both vertical and horizontal directions, indicating the surface-wave nature of eigenmodes.

APPENDIX B: INFLUENCE OF GEOMETRY PARAMETERS ON THE MAGNETIC HYPERBOLIC POLARITONS

We study the influence of different geometry parameters on the magnetic hyperbolic polaritons. As shown in Figs. 6(a) and 6(b), one can see that when enlarging the periodicity along the x or y axis (a or b), the bandwidth of the hyperbolic region (along k_y) decreases. The extremely large periodicity would lead

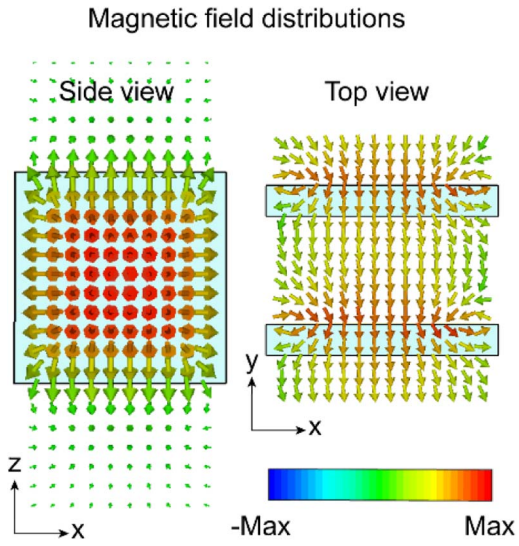

Fig. 5. Side and top views of magnetic field distributions of eigenmodes, respectively. The color bar measures the amplitude of the magnetic field.

to a flat band with a narrow bandwidth centered at the magnetic resonance frequency of a single isolated coil. We also study the relations between dispersions and number of turns of coils n, as shown in Fig. 6(c), which manifests the number of turns determines the frequency range of metasurface dispersions. In addition, the dispersions dramatically change when altering the substrate thickness t under 1.5 mm, while the dispersions almost keep the same when the thickness is larger than 1.5 mm [see Fig. 6(d)].

In our experiments, considering the convenience of fabrication and measurement, we choose the current geometry parameters as described in the main text. However, we would like to mention that the hyperbolic behavior of the designer polaritons over our designed metasurface is generally robust. Its existence is not sensitive to moderate parameter changes.

APPENDIX C: DERIVATION OF THE DISPERSIONS FROM AN ANISOTROPIC MAGNETIC SHEET CONDUCTIVITY

In this section, we analytically determine the dispersion relations of the designer polaritons on the hyperbolic metasurface. We assume the hyperbolic metasurface locates at $z = 0$ plane between region 1 (air, $z > 0$) and region 2 (air, $z < 0$). Note that the thickness of the metasurface is 15.2 mm, which is typically much smaller than the operational wavelength in free space (denoted as $\lambda_0 = 2 \times 10^3$ mm). Therefore, the hyperbolic metasurface can be considered as an ultra-thin uniaxial metasurface defined by the sheet conductivity:

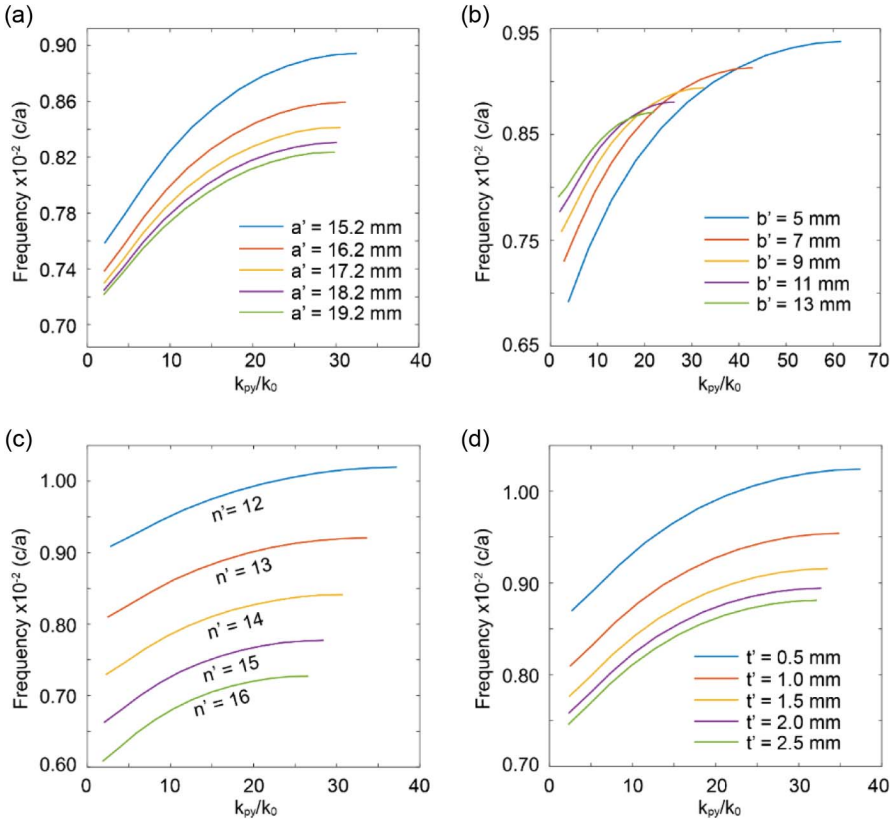

Fig. 6. Influence of different geometry parameters on the magnetic hyperbolic polaritons. (a) Dispersions of the metasurface with different periodicity along the x axis (a'). Other parameters keep constant, i.e., $b' = 9$ mm, $n' = 14$, and $t' = 2$ mm. (b) Dispersions of the metasurface with different periodicity along the y axis (b'). Other parameters keep constant, i.e., $a' = 15.2$ mm, $n' = 14$, and $t' = 2$ mm. (c) Dispersions of the metasurface with different number of turns of coils (n'). Other parameters keep constant, i.e., $a' = 15.2$ mm, $b' = 9$ mm, and $t' = 2$ mm. (d) Dispersions of the metasurface with different thickness (t'). Other parameters keep constant, i.e., $a' = 15.2$ mm, $b' = 9$ mm, and $n' = 14$.

$$\overline{\overline{\sigma}} = \begin{pmatrix} \sigma_{xx} & & \\ & \sigma_{yy} & \\ & & 0 \end{pmatrix}. \tag{C1}$$

For simplicity, we define a new $x'y'z$ coordinate system that is rotated by an angle φ on the xy plane comparing with the original xyz coordinate system, and the direction of the wave vector of the designer polaritons is x'. According to the kDB system, the sheet conductivity $\overline{\overline{\sigma}}'$ in the new coordinate system can be written as

$$\overline{\overline{\sigma}}' = \overline{\overline{T}} \cdot \overline{\overline{\sigma}} \cdot \overline{\overline{T}}^{-1}$$
$$= \begin{pmatrix} \sigma_{xx}\sin^2\varphi + \sigma_{yy}\cos^2\varphi & (\sigma_{xx} - \sigma_{yy})\sin\varphi\cos\varphi & 0 \\ (\sigma_{xx} - \sigma_{yy})\sin\varphi\cos\varphi & \sigma_{xx}\cos^2\varphi + \sigma_{yy}\sin^2\varphi & 0 \\ 0 & 0 & 0 \end{pmatrix},$$

where $\overline{\overline{T}} = \begin{pmatrix} \sin\varphi & -\cos\varphi & 0 \\ \cos\varphi & \sin\varphi & -\sin\varphi \\ 0 & 0 & 1 \end{pmatrix}$ and

$$\overline{\overline{T}}^{-1} = \begin{pmatrix} \sin\varphi & \cos\varphi & 0 \\ -\cos\varphi & \sin\varphi & 0 \\ 0 & 0 & 1 \end{pmatrix}. \tag{C2}$$

In the uniaxial metasurfaces, TM or TE modes simultaneously exist. However, TM modes here are barely confined on the metasurface; thus we mainly focus on TE modes in the $x'y'z$ coordinate system, whose field distributions in region 1 and region 2 can be written as

$$\begin{aligned} \overline{E_1} &= \hat{y}' e^{ik_{x'}x' + k_z z}, \\ \overline{H_1} &= \frac{1}{\omega\mu_0}(\hat{z}k_{x'} + \hat{x}' i k_z) e^{ik_{x'}x' + k_z z}, \\ \overline{E_2} &= \hat{y}' A e^{ik_{x'}x' - k_z z}, \\ \overline{H_2} &= \frac{A}{\omega\mu_0}(\hat{z}k_{x'} - \hat{x}' i k_z) e^{ik_{x'}x' - k_z z}, \end{aligned} \tag{C3}$$

where $k_z = \sqrt{k_{x'}^2 + k_{y'}^2 - k_0^2}$ is the imaginary part of the wave vector in the z axis, $k_{x',y'}$ are the wave vectors in the $x'y'$ plane, and k_0 is the wave vector in free space.

Then we extract the anisotropic magnetic sheet conductivity based on the following equation:

$$\sigma_m = 2\zeta \frac{1 + R - T}{1 - R + T}, \tag{C4}$$

where ζ is the wave impedance defined by $\zeta^{-1} = \frac{k_1}{\omega\mu_0}$, and R and T are the reflection and transmission coefficients, respectively [30]. The magnetic sheet conductivity $\overline{\overline{\sigma_m}}$ indicates there are two-dimensional magnetic sheet currents over the metasurface [30,31], so that the boundary conditions can be expressed by $\hat{n} \times (\overline{H_1} - \overline{H_2}) = 0$ and $\hat{n} \times (\overline{E_1} - \overline{E_2}) = -\overline{\overline{\sigma_m}} \cdot \overline{H}$, where $\hat{n} = -\hat{z}$. By solving the boundary conditions, we have

$$\frac{1}{\eta_0^2}(\sigma_{xx}\sin^2\varphi + \sigma_{yy}\cos^2\varphi)^2(k_x^2 + k_y^2 - k_0^2) + 4k_0^2 = 0, \tag{C5}$$

where η_0 is the characteristic impedance of vacuum. Substituting $\sin^2\varphi = \frac{k_x^2}{k_x^2 + k_y^2}$ and $\cos^2\varphi = \frac{k_y^2}{k_x^2 + k_y^2}$ into Eq. (C5), we obtain the dispersion relations of the hyperbolic designer polaritons:

$$\frac{1}{\eta_0^2}(\sigma_{xx}k_x^2 + \sigma_{yy}k_y^2)^2(k_x^2 + k_y^2 - k_0^2) + 4k_0^2(k_x^2 + k_y^2)^2 = 0. \tag{C6}$$

By substituting the retrieved magnetic sheet conductivity into Eq. (C6), we get the analytical IFCs of the hyperbolic designer polaritons from $0.735 \times 10^{-2}(c/a)$ to $0.835 \times 10^{-2}(c/a)$, as shown in Fig. 7(a). Figure 7(b) illustrates the simulated IFCs, which have a good agreement with the analytical results in the range of $[-0.5\pi/a, 0.5\pi/a] \times [-0.5\pi/b, 0.5\pi/b]$ that around the Brillouin zone center [45].

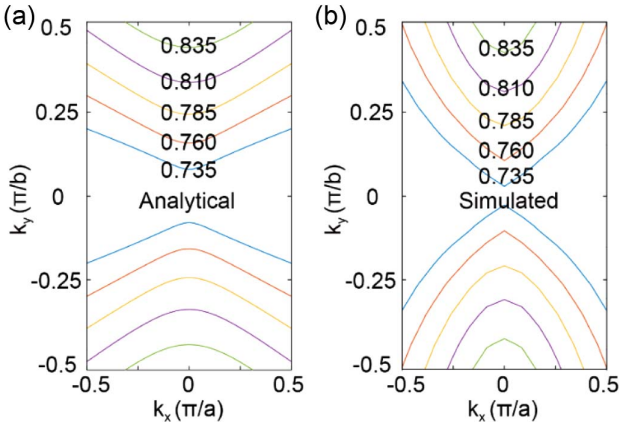

Fig. 7. Analytical and simulated iso-frequency contours. (a) Iso-frequency contours obtained from theoretical analysis. (b) Iso-frequency contours obtained from numerical simulations. The frequency values are normalized by $(c/a) \times 10^{-2}$.

APPENDIX D: ANALYSIS ON FIELD PATTERN

The measured momentum space at $0.765 \times 10^{-2}(c/a)$ is shown in Fig. 8(a). One can observe that only the modes with $k_x > 0$ are excited, which is consistent with the measured field pattern in Fig. 8(b). In addition, as our metasurface has mirror symmetry along the x direction (according to the effective medium theory), we can flip the x axis to obtain a field pattern shown in Fig. 8(c), which is similar to the standard hyperbola-like profile [14,25].

APPENDIX E: DESIGN OF A FAR-INFRARED HYPERBOLIC METASURFACE

In this section, we show a design of a hyperbolic metasurface working in the far-infrared regime. Figure 9(a) gives the schematic of the far-infrared hyperbolic metasurface, which consists of coiling silver wires with x-period $a = 1.9$ μm and y-period $b = 1.16$ μm. Figure 9(b) illustrates the details of a unit cell, where the yellow region represents the silver that is numerically described by the Drude model:

$$\varepsilon(\omega) = 1 - \frac{\omega_p^2}{\omega(\omega + i\nu)}, \tag{E1}$$

with the plasma frequency $\omega_p = 1.37 \times 10^{16}$ rad/s and collision frequency $\nu = 6.5 \times 10^{12}$ s^{-1}. We then obtain the

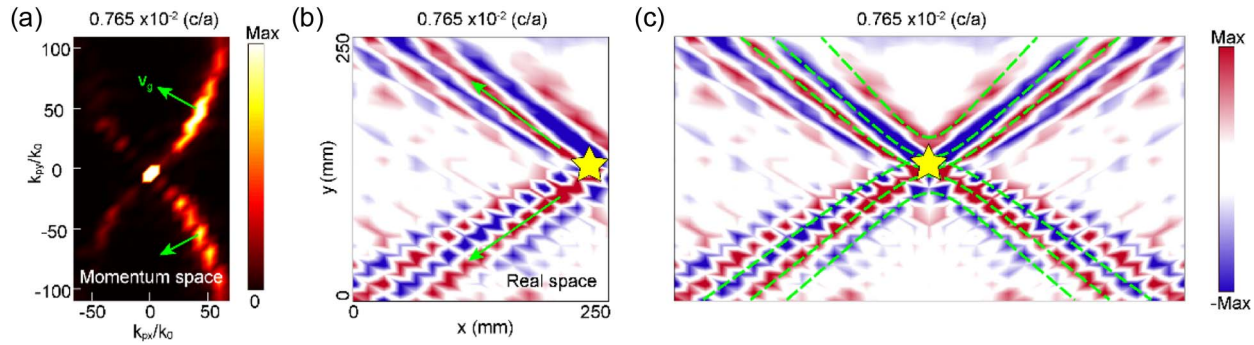

Fig. 8. (a) Measured momentum space at $0.765 \times 10^{-2}(c/a)$. The color bar measures the energy intensity. (b) Measured H_z field on the xy plane 3 mm over the hyperbolic metasurface at $0.765 \times 10^{-2}(c/a)$. The excitation is marked as a yellow star. Here, the green arrows in (a) and (b) depict the direction of group velocity (energy flow) of the high-k modes. (c) Measured H_z field by flipping the x axis of the field in (b). The green dashed curves depict the wavefronts of the hyperbolic polaritons. The color bar measures the real part of H_z.

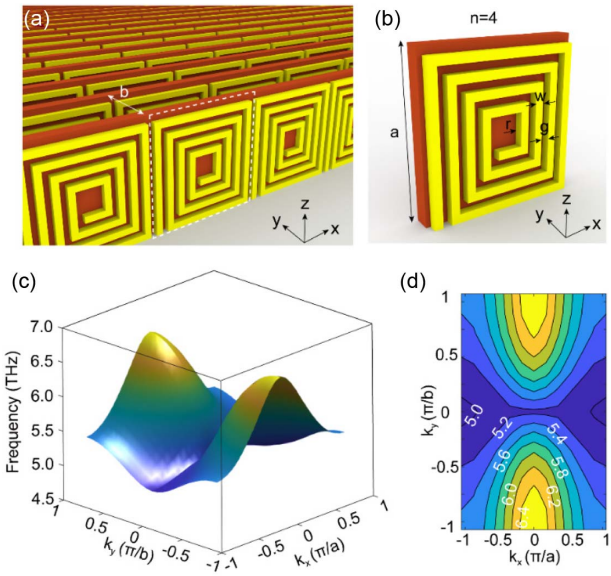

Fig. 9. Design of a far-infrared hyperbolic metasurface. (a) Schematic of a far-infrared hyperbolic metasurface consisting of coiling silver wires. Yellow area: coiling silver wires. White dashed line: a unit cell. Here, the brown area represents air in order to make the structure look clear. (b) Details of a unit cell. Here, $a = 1.9$ μm, $b = 1.16$ μm, $r = 0.2$ μm, $w = 0.1$ μm, and $g = 0.1$ μm. Number of coil turns is $n = 4$. The thickness of coiling silver wires is 0.1 μm. (c) Three-dimensional perspective view of the dispersion relations of the far-infrared hyperbolic metasurface in the first Brillouin zone. (d) Iso-frequency contours of the metasurface. The hyperbolic contours range from 5.0 to 6.4 THz. The frequency values are presented in the unit of terahertz.

dispersion relations and the corresponding IFCs of the far-infrared hyperbolic metasurface in the FBZ, as shown in Figs. 9(c) and 9(d), which indicate the convergent manners of the designer polaritons from 5.0 to 6.4 THz. In addition, our calculations show that the far-infrared hyperbolic metasurface has a high squeezing factor up to 27.3.

APPENDIX F: MATERIALS AND METHODS

1. Numerical Simulations

We use the eigenvalue module of a commercial software CST Microwave Studio to calculate the photonic band dispersions of the fundamental mode of the designed hyperbolic metasurface in the FBZ. The coiling copper wire is considered as a perfect electric conductor (PEC), and the substrate is regarded as a lossless medium. We apply the periodic boundary in the lateral direction. Note that there is no open boundary in the eigenvalue module; thus, we employ the PEC boundary in the z direction with 30-mm air above and below the structure, which is approximately equivalent to the open boundary. The eigenfrequencies of each wave vector obtained from CST will be imported into MATLAB to get the band dispersions.

2. Experimental Sample and Setup

We employ printed circuit board (PCB) technology to manufacture the experimental sample, which consists of one-side 35-μm coiling copper (dimensional tolerance ±0.1 mm) attached onto a 2-mm F4B PCB (relative permittivity 3.50 ± 0.05, and thickness tolerance ±0.05 mm). Note that we utilize three-dimensional printing technology to fabricate the resin structure [green structure in Fig. 10(a)] in order to sustain the hyperbolic metasurface, thus guaranteeing the in-plane periodicity.

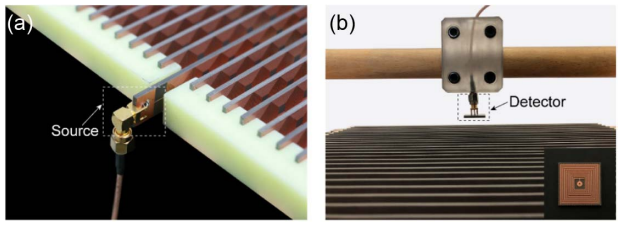

Fig. 10. Experimental setup. (a) A source, which is a broadband antenna, is directly welded on a coil unit cell at the metasurface edge. Green resin structure is used to sustain the hyperbolic metasurface. (b) A detector is a compact coil antenna with magnetic resonance around $0.806 \times 10^{-2}(c/a)$. The coil-like detector oriented in the direction, is fixed at a robotic arm of a moving platform and moves on the plane 3 mm above the designed hyperbolic metasurface. The inset represents the details of the detector.

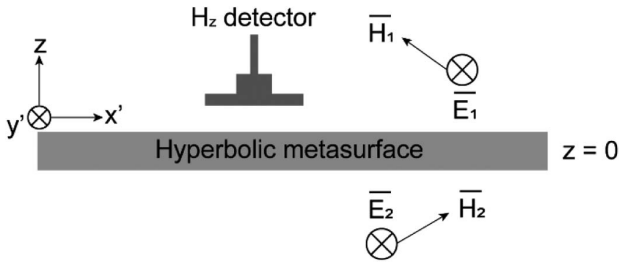

Fig. 11. Scheme view of the fields around the hyperbolic metasurface and the coil antenna as a detector.

The experimental setup is shown in Fig. 10, where a VNA collects the amplitude and phase of the measured magnetic field from a source and a detector. A broadband antenna is directly welded on a coil unit cell at the metasurface edge, serving as a source to excite the designer polaritons efficiently at the frequency within the hyperbolic region [46]. Here, the efficiency of the surface designer polariton excitation depends on the impedance matching between the source and the metasurface. In addition, in order to increase the transmissions, we design a compact coil antenna with magnetic resonance around $0.806 \times 10^{-2}(c/a)$ as a detector, which has the same geometric parameters as the unit cell except for the side length (i.e., 16 mm), as shown in Fig. 10(b). We note that the magnetic field has nonzero $H_{x'}$ and H_z components. Thus the coil-like detector is oriented in the z direction to measure the H_z field (see Fig. 11). The detector is fixed at a robotic arm of a moving platform 3 mm above the hyperbolic metasurface. A computer controls the speed and step of the moving platform while scanning the sample automatically. Here, we set the steps as 15.2 mm and 9 mm for the x and y directions, respectively, which are the same as the x- and y-periods, so that it simplifies the imaging process of spatial Fourier transform. By scanning the whole region of the designed hyperbolic metasurface, the complex magnetic patterns of H_z field are recorded.

Funding. National Natural Science Foundation of China (61625502, 61975176, 11961141010); Top-Notch Young Talents Program of China; Fundamental Research Funds for the Central Universities; Ministry of Education-Singapore (MOE2015-T2-1-070, MOE2016-T3-1-006, MOE2018-T2-1-022 (S), Tier 1 RG174/16 (S)).

Disclosures. The authors declare no conflicts of interest.

Data Availability. Data underlying the results presented in this paper are not publicly available at this time but may be obtained from the authors upon reasonable request.

REFERENCES

1. D. R. Smith and D. Schurig, "Electromagnetic wave propagation in media with indefinite permittivity and permeability tensors," Phys. Rev. Lett. **90**, 077405 (2003).
2. Z. Jacob, J.-Y. Kim, G. V. Naik, A. Boltasseva, E. E. Narimanov, and V. M. Shalaev, "Engineering photonic density of states using metamaterials," Appl. Phys. B **100**, 215–218 (2010).
3. H. N. S. Krishnamoorthy, Z. Jacob, E. Narimanov, I. Kretzschmar, and V. M. Menon, "Topological transitions in metamaterials," Science **336**, 205–209 (2012).
4. A. Poddubny, I. Iorsh, P. Belov, and Y. Kivshar, "Hyperbolic metamaterials," Nat. Photonics **7**, 948–957 (2013).
5. L. Ferrari, C. Wu, D. Lepage, X. Zhang, and Z. Liu, "Hyperbolic metamaterials and their applications," Prog. Quantum. Electron. **40**, 1–40 (2015).
6. P. Huo, S. Zhang, Y. Liang, Y. Lu, and T. Xu, "Hyperbolic metamaterials and metasurfaces: fundamentals and applications," Adv. Opt. Mater. **7**, 1801616 (2019).
7. F. Liu, L. Xiao, Y. Ye, M. Wang, K. Cui, X. Feng, W. Zhang, and Y. Huang, "Integrated Cherenkov radiation emitter eliminating the electron velocity threshold," Nat. Photonics **11**, 289–292 (2017).
8. H. Hu, X. Lin, J. Zhang, D. Liu, P. Genevet, B. Zhang, and Y. Luo, "Nonlocality induced Cherenkov threshold," Laser Photonics Rev. **14**, 2000149 (2020).
9. D. Lu, J. J. Kan, E. E. Fullerton, and Z. Liu, "Enhancing spontaneous emission rates of molecules using nanopatterned multilayer hyperbolic metamaterials," Nat. Nanotechnol. **9**, 48–53 (2014).
10. Y. Guo, C. L. Cortes, S. Molesky, and Z. Jacob, "Broadband super-Planckian thermal emission from hyperbolic metamaterials," Appl. Phys. Lett. **101**, 131106 (2012).
11. S. A. Biehs, M. Tschikin, R. Messina, and P. B. Abdallah, "Super-Planckian near-field thermal emission with phonon-polaritonic hyperbolic metamaterials," Appl. Phys. Lett. **102**, 131106 (2013).
12. K. V. Sreekanth, Y. Alapan, M. ElKabbash, E. Ilker, M. Hinczewski, U. A. Gurkan, A. De Luca, and G. Strangi, "Extreme sensitivity biosensing platform based on hyperbolic metamaterials," Nat. Mater. **15**, 621–627 (2016).
13. Z. Liu, H. Lee, Y. Xiong, C. Sun, and X. Zhang, "Far-field optical hyperlens magnifying sub-diffraction-limited objects," Science **315**, 1686 (2007).
14. P. Li, I. Dolado, F. J. Alfaro-Mozaz, F. Casanova, L. E. Hueso, S. Liu, J. H. Edgar, A. Y. Nikitin, S. Vélez, and R. Hillenbrand, "Infrared hyperbolic metasurface based on nanostructured van der Waals materials," Science **359**, 892–896 (2018).
15. Y. Liu and X. Zhang, "Metasurfaces for manipulating surface plasmons," Appl. Phys. Lett. **103**, 141101 (2013).
16. A. A. High, R. C. Devlin, A. Dibos, M. Polking, D. S. Wild, J. Perczel, N. P. de Leon, M. D. Lukin, and H. Park, "Visible-frequency hyperbolic metasurface," Nature **522**, 192–196 (2015).
17. Y. Yang, L. Jing, L. Shen, Z. Wang, B. Zheng, H. Wang, E. Li, N.-H. Shen, T. Koschny, C. M. Soukoulis, and H. Chen, "Hyperbolic spoof plasmonic metasurfaces," NPG Asia Mater. **9**, e428 (2017).
18. Y. Yang, P. Qin, B. Zheng, L. Shen, H. Wang, Z. Wang, E. Li, R. Singh, and H. Chen, "Magnetic hyperbolic metasurface: concept, design, and applications," Adv. Sci. **5**, 1801495 (2018).
19. Y. Yang, P. Qin, X. Lin, E. Li, Z. Wang, B. Zhang, and H. Chen, "Type-I hyperbolic metasurfaces for highly squeezed designer polaritons with negative group velocity," Nat. Commun. **10**, 2002 (2019).
20. T. Low, A. Chaves, J. D. Caldwell, A. Kumar, N. X. Fang, P. Avouris, T. F. Heinz, F. Guinea, L. Martin-Moreno, and F. Koppens, "Polaritons in layered two-dimensional materials," Nat. Mater. **16**, 182–194 (2017).
21. S. Dai, Z. Fei, Q. Ma, A. S. Rodin, M. Wagner, A. S. McLeod, M. K. Liu, W. Gannett, W. Regan, K. Watanabe, T. Taniguchi, M. Thiemens, G. Dominguez, A. H. C. Neto, A. Zettl, F. Keilmann, P. Jarillo-Herrero, M. M. Fogler, and D. N. Basov, "Tunable phonon polaritons in atomically thin van der Waals crystals of boron nitride," Science **343**, 1125–1129 (2014).
22. S. Dai, Q. Ma, M. K. Liu, T. Andersen, Z. Fei, M. D. Goldflam, M. Wagner, K. Watanabe, T. Taniguchi, M. Thiemens, F. Keilmann, G. C. A. M. Janssen, S.-E. Zhu, P. Jarillo-Herrero, M. M. Fogler, and D. N. Basov, "Graphene on hexagonal boron nitride as a tunable hyperbolic metamaterial," Nat. Nanotechnol. **10**, 682–686 (2015).
23. P. Li, M. Lewin, A. V. Kretinin, J. D. Caldwell, K. S. Novoselov, T. Taniguchi, K. Watanabe, F. Gaussmann, and T. Taubner, "Hyperbolic phonon-polaritons in boron nitride for near-field optical imaging and focusing," Nat. Commun. **6**, 7507 (2015).

24. W. Ma, P. Alonso-González, S. Li, A. Y. Nikitin, J. Yuan, J. Martín-Sánchez, J. Taboada-Gutiérrez, I. Amenabar, P. Li, S. Vélez, C. Tollan, Z. Dai, Y. Zhang, S. Sriram, K. Kalantar-Zadeh, S.-T. Lee, R. Hillenbrand, and Q. Bao, "In-plane anisotropic and ultra-low-loss polaritons in a natural van der Waals crystal," Nature **562**, 557–562 (2018).
25. Z. Zheng, N. Xu, S. L. Oscurato, M. Tamagnone, F. Sun, Y. Jiang, Y. Ke, J. Chen, W. Huang, W. L. Wilson, A. Ambrosio, S. Deng, and H. Chen, "A mid-infrared biaxial hyperbolic van der Waals crystal," Sci. Adv. **5**, eaav8690 (2019).
26. J. S. Gomez-Diaz and A. Alù, "Flatland optics with hyperbolic metasurfaces," ACS Photonics **3**, 2211–2224 (2016).
27. X. Lin, Y. Yang, N. Rivera, J. J. López, Y. Shen, I. Kaminer, H. Chen, B. Zhang, J. D. Joannopoulos, and M. Soljačić, "All-angle negative refraction of highly squeezed plasmon and phonon polaritons in graphene-boron nitride heterostructures," Proc. Natl. Acad. Sci. USA **114**, 6717–6721 (2017).
28. J. Jiang, X. Lin, and B. Zhang, "Broadband negative refraction of highly squeezed hyperbolic polaritons in 2D materials," Research **2018**, 2532819 (2018).
29. J. Elser and V. A. Podolskiy, "Scattering-free plasmonic optics with anisotropic metamaterials," Phys. Rev. Lett. **100**, 066402 (2008).
30. P. Tassin, T. Koschny, and C. M. Soukoulis, "Effective material parameter retrieval for thin sheets: theory and application to graphene, thin silver films, and single-layer metamaterials," Phys. B **407**, 4062–4065 (2012).
31. M. Albooyeh, D. H. Kwon, F. Capolino, and S. A. Tretyakov, "Equivalent realizations of reciprocal metasurfaces: role of tangential and normal polarization," Phys. Rev. B **95**, 115435 (2017).
32. A. V. Kildishev, A. Boltasseva, and V. M. Shalaev, "Planar photonics with metasurfaces," Science **339**, 1232009 (2013).
33. J. S. Gomez-Diaz, M. Tymchenko, and A. Alù, "Hyperbolic plasmons and topological transitions over uniaxial metasurfaces," Phys. Rev. Lett. **114**, 233901 (2015).
34. O. Y. Yermakov, A. I. Ovcharenko, M. Song, A. A. Bogdanov, I. V. Iorsh, and Y. S. Kivshar, "Hybrid waves localized at hyperbolic metasurfaces," Phys. Rev. B **91**, 235423 (2015).
35. A. Nemilentsau, T. Low, and G. Hanson, "Anisotropic 2D materials for tunable hyperbolic plasmonics," Phys. Rev. Lett. **116**, 066804 (2016).
36. C. Luo, S. G. Johnson, J. Joannopoulos, and J. Pendry, "All-angle negative refraction without negative effective index," Phys. Rev. B **65**, 201104 (2002).
37. H. Shin and S. Fan, "All-angle negative refraction for surface plasmon waves using a metal-dielectric-metal structure," Phys. Rev. Lett. **96**, 073907 (2006).
38. G. Hu, A. Krasnok, Y. Mazor, C. W. Qiu, and A. Alù, "Moiré hyperbolic metasurfaces," Nano Lett. **20**, 3217–3224 (2020).
39. Z. Zheng, F. Sun, W. Huang, J. Jiang, R. Zhan, Y. Ke, H. Chen, and S. Deng, "Phonon polaritons in twisted double-layers of hyperbolic van der Waals crystals," Nano Lett. **20**, 5301–5308 (2020).
40. J. Duan, N. Capote-Robayna, J. Taboada-Gutiérrez, G. Álvarez-Pérez, I. Prieto, J. Martín-Sánchez, A. Y. Nikitin, and P. Alonso-González, "Twisted nano-optics: manipulating light at the nanoscale with twisted phonon polaritonic slabs," Nano Lett. **20**, 5323–5329 (2020).
41. G. Hu, Q. Ou, G. Si, Y. Wu, J. Wu, Z. Dai, A. Krasnok, Y. Mazor, Q. Zhang, Q. Bao, C.-W. Qiu, and A. Alù, "Topological polaritons and photonic magic angles in twisted α-MoO_3 bilayers," Nature **582**, 209–213 (2020).
42. M. Chen, X. Lin, T. H. Dinh, Z. Zheng, J. Shen, Q. Ma, H. Chen, P. Jarillo-Herrero, and S. Dai, "Configurable phonon polaritons in twisted α-MoO_3," Nat. Mater. **19**, 1307–1311 (2020).
43. J. Zhang, X. Hu, H. Chen, and F. Gao, "Designer surface plasmons enable terahertz Cherenkov radiation," Prog. Electromagn. Res. **169**, 25–32 (2020).
44. X. Yao, S. Li, and S. He, "Dual-mode hyperspectral bio-imager with a conjugated camera for quick object-selection and focusing," Prog. Electromagn. Res. **168**, 133–143 (2020).
45. M. Mahmoodi, S. H. Tavassoli, O. Takayama, J. Sukham, R. Malureanu, and A. V. Lavrinenko, "Existence conditions of high-*k* modes in finite hyperbolic metamaterials," Laser Photonics Rev. **13**, 1800253 (2019).
46. A. Nemilentsau, T. Stauber, G. Gómez-Santos, M. Luskin, and T. Low, "Switchable and unidirectional plasmonic beacons in hyperbolic two-dimensional materials," Phys. Rev. B **99**, 201405(R) (2019).